Medium modifications of antikaons in dense matter

Th. Roth[a], M. Buballa[a], and J. Wambach[a,b]

[a] *Institut für Kernphysik, TU Darmstadt,*

Schlossgartenstr. 9, D-64289 Darmstadt, Germany

[b] *Gesellschaft für Schwerionenforschung (GSI),*

Planckstr. 1, D-64291 Darmstadt, Germany

Abstract

We investigate the modification of antikaons in isospin symmetric and asymmetric nuclear matter. Using the leading s–wave couplings of the SU(3) chiral meson–baryon Lagrangian we solve the coupled channel kaon–nucleon scattering equation selfconsistently. The in–medium antikaon propagator is calculated for different densities and different proton/neutron ratios. The spectral function of the antikaon is found to be broadened strongly, and its mass is shifted downward significantly. However, comparing the effective in–medium mass of the antikaon to the relevant charge chemical potential of neutron star matter, we find that kaon condensation is unlikely to occur in neutron stars.

1 Introduction

Understanding the properties of strongly interacting matter under extreme conditions such as high temperatures or densities is of considerable interest in hadronic physics. In this context strange particles play a key role. In ultrarelativistic heavy–ion collisions, primarily exploring the high–temperature regime of the QCD phase diagram, strangeness enhancement is considered to be one of the possible signals for the formation of the quark–gluon plasma [1]. At low temperatures but high densities, as present, e.g., in the interiors of neutron stars, strangeness might show up in the form of a condensate of negative kaons. This possibility was first pointed out by Kaplan and Nelson [2, 3] and has received great attention since. The appearance of an antikaon condensate would soften the equation of state of the star, allowing more compact stellar objects.

The basic considerations leading to this idea are relatively simple [4]: Since kaons, as the lightest mesons with strangeness, are the (pseudo–) Goldstone bosons of $SU(3)$ chiral symmetry breaking, their interactions can be studied within chiral perturbation theory (χPT). At lowest order, the corresponding kaon–nucleon scattering Lagrangian contains two s–wave interaction terms: a constant scalar term due to explicit chiral symmetry breaking and a momentum–dependent vector term, the so–called Weinberg–Tomozawa term [5, 6]. The scalar interaction is attractive for both, kaons and antikaons, while the

vector interaction is repulsive for kaons (K^+ and K^0) but attractive for antikaons (K^- and $\bar{K}^0$). As a result, one expects an interaction which at tree level is weakly repulsive for kaons but strongly attractive for antikaons. Hence, despite large quantitative uncertainties, the antikaon mass should decrease in matter, eventually leading to kaon condensation, once the mass drops below the chemical potential of the surrounding leptons.

Unfortunately, the situation is not that simple. Firstly, it should be noted that there is an ongoing controversial discussion about possible ambiguities related to the off–shell extrapolation from the $\overline{K}N$–scattering amplitude to the kaon selfenergy [7, 8, 9, 10]. Moreover, the empirical value of the s–wave K^- nucleon scattering length is *repulsive* at threshold ($\Re e\, a_{K^-p} = -0.78$ fm). This discrepancy between experiment and the above considerations can be attributed to the existence of the $\Lambda(1405)$ resonance just below the KN threshold, which gives rise to a repulsive contribution to the scattering amplitude at threshold. Apart from a few exceptions where the $\Lambda(1405)$ has been introduced as an elementary field [11], in most models it is dynamically generated through the $\overline{K}N$ – scattering process [12, 13, 14, 15]. In this case it cannot be treated perturbatively.

On the other hand, there are various experimental indications that antikaons, once they propagate through dense nuclear matter, indeed feel an attractive potential. Studies of the energy shifts and the widths of the lowest levels in kaonic atoms probe the behavior of antikaons in nuclear matter of densities between zero and ρ_0. A collection of data over a wide range of atoms was analyzed by Friedman [16]. These results require an attractive potential for the antikaons, although different theoretical approaches lead to quite different values for the depth of this potential [17, 18].

This finding is supported by the kaon data in heavy–ion collisions. The azimuthal emission patterns of K^+ and K^- obtained by the FOPI and KaoS collaborations [19, 20] indicate a different in–medium behavior for kaons and antikaons, corresponding to repulsive and attractive interactions, respectively. Naively, this also gives a simple explanation for the enhanced K^-/K^+ ratios which are found in nucleus–nucleus collisions as compared with (anti–) kaon production in NN: Lowering the K^- mass would reduce its production threshold and thus increase the yield [21, 22, 23]. However, the situation is complicated by the fact that in dense matter the K^- yield is enhanced, even without medium modification of its mass. This is because there are hyperons around (e.g., owing to prior K^+ production) which enable secondary production mechanisms, as $\pi Y \to K^- N$. Hence, for a consistent interpretation of the data, we do not only need a good understanding of the in–medium modification of the (anti–) kaons, but also of the above production process.

It is exactly this coupling of πY to $\overline{K}N$ that turns out to be the key to the interaction of the $\overline{K}$ with matter, giving rise to the $\Lambda(1405)$ resonance. This situation requires the treatment in terms of coupled channels, leading to the $\Lambda(1405)$ resonance and connected effects. Performing the coupled channel calculation at finite density results in a $\Lambda(1405)$ that is shifted upwards in energy [12, 13, 24, 25]. At lower energies around the original (vacuum) threshold the optical potential for the K^- becomes attractive, which would explain the data from kaonic atoms.

Still, one has to be careful with this kind of analysis. In the first works that went beyond a mean field description to include the $\Lambda(1405)$ (e.g. [12, 13, 24]), the repercussion of the dynamics of the $\Lambda(1405)$ on the antikaons were not included selfconsistently. However, this turned out to be of great importance: The selfconsistent $\Lambda(1405)$ does not

move very much [17, 14, 26], rendering the argument for the kaonic atoms questionable. Obviously, a comprehensive treatment of all the effects becomes necessary. This is what we aim at in this work. To this end, we basically carry out the following program, which is sketched in Fig. 1:

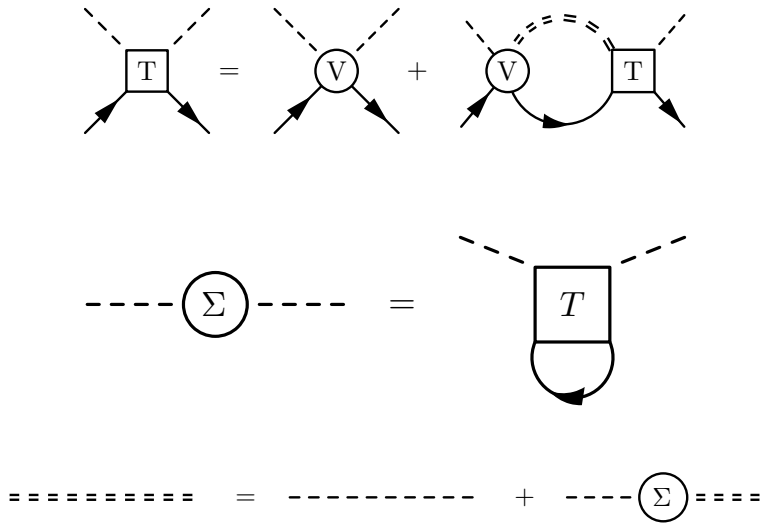

Figure 1: Illustration of the selfconsistency scheme: Scattering equation for the antikaon–nucleon T matrix (upper line), in–medium antikaon self–energy (center), and dressed kaon propagator (lower line).

In a first step we construct the $\overline{K}N$ T–matrix, taking into account the coupling of $\overline{K}N$ to all other important channels. Here the Lagrangian of chiral perturbation theory provides the basic interaction, i.e., the scattering kernel for the various mesons and baryons we take into account. As already indicated, the $\Lambda(1405)$ appears slightly (about 30 MeV) below the $\overline{K}N$ threshold which prohibits a purely perturbative treatment of the scattering process. Instead, we take the simplest diagram formed from $\mathcal{L}_{\chi PT}$ as the kernel of the Bethe–Salpeter scattering equation, sum it to all orders and get the $\Lambda(1405)$ as a dynamically generated resonance. In this context the coupling to other meson–baryon channels, in particular the $\pi\Sigma$ channel, which opens about 70 MeV below the resonance, is crucial.

Having constructed the scattering amplitudes in vacuum, we take the calculation to the dense medium, replacing the vacuum propagators by in–medium ones. The in–medium self–energy of the antikaon can be obtained from the T–matrix by closing a nucleon (hole) loop (see Fig. 1). This leads to a modified kaon propagator which, in turn, should be used to calculate the T–matrix. This procedure has to be iterated until a selfconsistent result is achieved.

A very important aspect in our calculations is the consideration of the momentum dependence of all calculated quantities. Calculating the antikaon selfenergy from the

in–medium scattering T–matrix means an integration over momentum, so the T–matrix, depending on energy and momentum separately in the medium, has to be known as a function of energy and momentum. This requirement becomes even stronger once we iterate the procedure to selfconsistency.

This is not just a technical issue. In general the existence of the nuclear matter rest frame as a preferred frame of reference forces us to specify explicitly the energy and momentum dependence of in–medium properties. In addition, considering heavy–ion collisions, the optical potential of the antikaon is probed at finite momentum. At a moderate temperature of $T = 80$ MeV [19] the antikaon has an average momentum of more than 300 MeV with respect to the matter rest frame. Momenta above ~ 300 MeV are typical in the experimental data on heavy ion collisions. Nevertheless, in many calculations it has been assumed that the attractive potential for the antikaons, i.e. their change in the mass is independent of momentum [13, 27]. This is not justified. To the contrary, a considerable momentum dependence of all in–medium properties is found [25], see also section 3.2.

In this article we focus on s–wave interactions. Kaon condensation is thus connected to the propagator at zero momentum. p–wave antikaon condensation has been investigated elsewhere [28, 29, 30, 31, 32, 33]. One aspect here is the effect of hyperon–nucleon–hole contributions on the antikaon selfenergy. We briefly investigate these contributions in Sect. 3.4. As they turn out to be very small, but would lead to considerable technical complications, we carry out the selfconsistency problem with the s–wave part alone.

The remainder of this work is organized as follows. In Sect. 2, we briefly discuss the formalism involved in calculating the $SU(3)$ meson–baryon scattering in a coupled channels scheme, based on the χPT Lagrangian. After that, in Sect. 3, the model is used to investigate the behavior of antikaons in dense isospin symmetric matter. Among other aspects we study the effect of the selfconsistent treatment, the momentum and density dependence of the propagator, and the role of the in–medium modification of pions. In Sect. 4 the analysis is extended to isospin asymmetric matter, i.e., to systems with different densities of protons and neutrons, as found in realistic systems. The implications of these results for the question of antikaon condensation in neutron stars are discussed Sect. 5. Our main results are summarized in Sect. 6.

2 Meson–baryon scattering

As outlined above (see Fig. 1), the first step in our procedure to construct the in–medium kaon propagator consists in a coupled–channel calculation of the $\bar{K}N \to \bar{K}N$ scattering amplitude,

$$\langle \overline{K}(k')\, N(p')|\, T\, |\overline{K}(k)\, N(p)\rangle \;=\; (2\pi)^4\, \delta^4(k'+p'-k-p)\, \overline{u}(p') T_{KN\to KN}(k',p';k,p)\, u(p)\,. \quad (1)$$

The T matrix elements are given by the Bethe–Salpeter equation [34],

$$T_{fi} \;=\; V_{fi} \;+\; \sum_c \int \frac{d^4l}{(2\pi)^4} V_{fc}\, \mathcal{G}_c^{BS}\, T_{ci}\;, \quad (2)$$

which is graphically sketched in the upper line of Fig. 1. We will refer to this equation also as the T–matrix equation. The indices i and f denote the incoming and outgoing meson–baryon channels, while the index c indicates the intermediate states, i.e., the meson–baryon channels that form the loop. For brevity we have suppressed all momentum arguments and only kept the loop momentum l.

Input to the T–matrix equation are the interaction kernel V, which will be specified in Sect. 2.1, and the two–particle propagator $\mathcal{G}^{BS}$. The latter is basically the product of the single–particle propagators of the baryon B_c and the meson M_c in the loop, $\mathcal{G}_c^{BS} = i\, S_{B_c} G_{M_c}$. In this work we include all channels of the SU(3) meson and baryon octets coupled to total strangeness -1, dropping the Ξ–channels that open only at larger energies.

2.1 Interaction

As discussed earlier, the interaction kernel V which enters the T–matrix equation is derived from the $SU(3)$ chiral Lagrangian. The basic building blocks are the matrices

$$u \;=\; \exp\left(\frac{i\Phi}{f_\pi}\right) , \qquad \Phi = \frac{1}{\sqrt{2}} \begin{pmatrix} \frac{\eta}{\sqrt{6}} + \frac{\pi^0}{\sqrt{2}} & \pi^+ & K^+ \\ \pi^- & \frac{\eta}{\sqrt{6}} - \frac{\pi^0}{\sqrt{2}} & K^0 \\ K^- & \overline{K^0} & -\frac{2\eta}{\sqrt{6}} \end{pmatrix} , \tag{3}$$

and

$$B = \begin{pmatrix} \frac{1}{\sqrt{6}}\Lambda + \frac{1}{\sqrt{2}}\Sigma^0 & \Sigma^+ & p \\ \Sigma^- & \frac{1}{\sqrt{6}}\Lambda - \frac{1}{\sqrt{2}}\Sigma^0 & n \\ \Xi^- & \Xi^0 & -\sqrt{\frac{2}{3}}\Lambda \end{pmatrix} , \tag{4}$$

corresponding to the pseudoscalar meson and baryon octets, respectively.

At lowest chiral order, the Lagrangian contains two meson–baryon interaction terms:

$$\mathcal{L}_{MB}^{(1)} \;=\; \mathcal{L}_{WT} \;+\; \mathcal{L}_{pw} \; . \tag{5}$$

The first term,

$$\mathcal{L}_{WT} \;=\; i\, tr(\overline{B}\gamma^\mu[\Gamma_\mu, B]) \; , \qquad \text{with} \quad \Gamma_\mu = \frac{1}{2}(u^\dagger\partial_\mu u + u\partial_\mu u^\dagger) \; , \tag{6}$$

is the already mentioned Weinberg–Tomozawa term, which corresponds to s–wave interaction. As pointed out in the Introduction, this term is crucial for a realistic description of $\overline{K}N$ scattering and will give a main contribution to the interaction kernel.

The second term, $\mathcal{L}_{pw}$, corresponds to p–wave interactions. As we will show in Sect. 3.4 , it has only little effect in the $\overline{K}N$ sector. Of course, p–wave interactions must be included to describe medium modifications of *pions*. However, since pions are not selfconsistently coupled to the kaon sector in our model, they can be treated separately. This will be briefly discussed in Sect. 2.4.

At second chiral order there are three interaction terms due to explicit chiral symmetry breaking through the quark mass matrix $\mathcal{M} = diag(m_u, m_d, m_s)$. These are the "Sigma terms" [35, 36, 37], which are given by

$$\mathcal{L}_\Sigma = b_D\, tr(\overline{B}\{\chi_+, B\}) \;+\; b_F\, tr(\overline{B}[\chi_+, B]) \;+\; b_o\, tr(\overline{B}B)\, tr(\chi_+) \; , \tag{7}$$

with

$$\chi_+ \;=\; 2B_0(u^\dagger \mathcal{M}\, u^\dagger \,+\, u\, \mathcal{M}\, u) \;. \tag{8}$$

Although of higher chiral order, they are comparable in strength to the Weinberg–Tomozawa contribution when evaluated at the respective meson–baryon thresholds. Therefore they should be taken into account.

While B_0 can be related to the chiral condensate via the Gell–Mann–Oakes–Renner relation, $B_0 = -\langle\bar{q}q\rangle/f_\pi^2$, the constants b_D, b_F and b_0 are examples of the so called low–energy–constants (LECs). These parameters are not constrained by symmetries and have to be fixed from phenomenology. One can use the predictions of the theory for the baryon masses to pin down the values of at least b_D and b_F. The values used for the calculations in this work are taken from [38]:

$$b_D \;=\; 0.061 \text{ GeV}^{-1}, \qquad b_F \;=\; 0.195 \text{ GeV}^{-1}, \qquad b_0 \;=\; -0.346 \text{ GeV}^{-1} \;. \tag{9}$$

2.2 Factorization of the T–matrix equation

The difficult point in solving the Bethe–Salpeter equation, Eq. (2), is any momentum dependence in the vertices. For constant interaction kernels V, the equation can be factorized and reduces to a simple matrix equation which can straightforwardly be solved by inversion:

$$T \;=\; V \,+\, V\, J\, T \quad \Rightarrow \quad T \;=\; (1 - V\, J)^{-1}\, V \;. \tag{10}$$

Here J is a diagonal matrix in the space of meson–baryon channels c corresponding to the loop integrals

$$J_c \;=\; i \int \frac{d^4l}{(2\pi)^4}\, S_{B_c}\, G_{M_c} \;. \tag{11}$$

It depends on the total 4–momentum of the pair only and, hence, as long as V is constant, the T matrix also depends only on the total 4–momentum of the meson–baryon system.

However, in our case, V is not constant, because the Weinberg–Tomozawa term, Eq. (6), leads to 4–momentum dependent vertices via the derivatives ∂_μ. To avoid this difficulty we follow the commonly used strategy which involves the following approximations: First, we evaluate $\mathcal{L}_{WT}$ in the baryon rest frame [38, 15]. This amounts to replacing

$$\mathcal{L}_{WT} \;\rightarrow\; i\, tr(B^\dagger\, [\Gamma^0, B]) \;, \tag{12}$$

which removes the 3–momentum dependence. Still, the vertices depend on the energies k^0 and k'^0 of the incoming and outgoing meson fields, respectively, i.e.

$$V_{WT} \;\propto\; \frac{i}{2f_\pi}\,(k^0 + k'^0) \;. \tag{13}$$

Therefore we solve the T–matrix equation by applying the so–called on–shell factorization [38]. In practical terms this means that the T–matrix is calculated as in Eq. (10), and only in the final expression V is taken to depend on the energies k^0 and k'^0 of the external mesons. This approximation can be justified by the observation that any effect of the energy dependence of the vertices inside the loops can be absorbed in renormalization

constants and does not influence the on–shell part of the T–matrix which is related to the physical amplitudes, Eq. 1. For a more detailed discussion of these issues, see Refs. [7, 8, 9, 10, 38, 39, 40].

As a result of the above procedure, the problem reduces to the multiplication and inversion of matrices spanned by the various meson–baryon channels. Conceptually, this is of course much easier than solving the original Bethe–Salpeter equation. Nevertheless, owing to the coupling of the various meson–baryon channels, the expressions for the T–matrix elements in terms of the vertex– and loop matrices V and J comprise several thousand terms each, and thus will not be given here explicitly.

2.3 Regularization

We regularize the loop integral by employing twice subtracted dispersion relations in the calculation of its real part. The subtraction parameters can be fixed by fitting the resulting scattering amplitudes to the empirical scattering lengths [41, 42].

This approach has some advantage over the use of cut–offs or form factors: On the one hand, it keeps the vacuum–amplitude Lorentz–invariant. On the other hand it helps to overcome a technical problem of the selfconsistency procedure we aim at: Iteratively using the scattering matrix and the modified antikaon propagator as mutual input (see Fig. 1) requires the knowledge of these functions on infinite energy and momentum intervals. At large momenta, the antikaon propagator can be approximated by the free one. However, it is not immediately clear how to treat the scattering amplitude in that respect. Use of a cut–off will introduce artificial peaks into the T–matrix, especially at higher energies and momenta. This is not the case for the amplitude obtained by a twice subtracted dispersion relation, which is smooth enough to be restricted to a finite interval as well.

We find that our vacuum scattering amplitudes are in good agreement with the $\overline{K}N$ amplitudes of [38].

2.4 Pion–nucleon interaction

The formulation of the $\overline{K}N$ scattering problem in terms of coupled meson–baryon channels is the key ingredient of our model. In particular, the $\Lambda(1405)$ will only arise as a dynamically generated resonance if the $\overline{K}N$ channel is coupled to the $\pi\Sigma$ channel. Consequently, the in–medium amplitude will feel any medium–modifications of the pion.

The behavior of the pion in dense matter has been studied in great detail. The main sources of the pion selfenergy are particle–hole and delta ($\Delta(1232)$)–hole excitations. To capture these and other important features, in the pion sector we do not stick to the Lagrangian set up in Sect. 2.1 but include additional phenomenological terms which are taken from the literature. Here we basically follow Ref. [43].

The p–wave pion–nucleon interaction can be obtained from $\mathcal{L}_{pw}$ in Eq. (5). It is given by

$$\mathcal{L}_{\pi N} \;=\; \frac{f_N}{m_\pi}\,\bar{\psi}\,\gamma^5\,\gamma^\mu\;\vec{\tau}\,\psi\;\cdot\;\partial_\mu\,\vec{\phi}, \tag{14}$$

with the pseudovector coupling constant $f_N = 1.01$.

The coupling to the Δ looks quite similar:

$$\mathcal{L}_{\pi N\Delta} = -\frac{f_\Delta}{m_\pi}\bar{\psi}\vec{T}^\dagger\psi_\mu \cdot \partial^\mu\vec{\phi} \quad + \quad \text{h. c.} \tag{15}$$

Both, the πNN and $\pi N\Delta$ vertices, are supplemented by a monopole form factor

$$\Gamma_\pi(\vec{k}) = \frac{\Lambda^2}{\Lambda^2 + \vec{k}^2} \ , \tag{16}$$

with $\Lambda = 550$MeV. Finally, short–range correlations are taken into account via Migdal parameters $g'_{NN} = 0.8$ and $g'_{N\Delta} = g'_{\Delta\Delta} = 0.5$. No indications for p–wave pion condensation are observed for the densities considered here (up to $5\rho_0$).

Having calculated the pion propagator in dense matter, this propagator is put into the loops with the Λ and Σ baryons. These loops are then coupled to the other meson–baryon channels to obtain the T–matrix element. As pointed out before, we do not further modify the pion itself, i.e., we do not aim for selfconsistency in the case of the pion. This is justified because the above model of the pion [43, 44, 45, 46] is already designed to give a realistic result as it stands, without further iteration.

3 The kaon propagator in symmetric nuclear matter

We can now proceed to calculate the in–medium antikaon propagator following the self-consistent scheme outlined in the Fig. 1.

A typical example for the resulting antikaon selfenergy is given in the upper panel of Fig. 2, where the real and imaginary parts of Σ_K at normal nuclear matter density, $\rho = \rho_0 = 0.16$ fm^{-3}, are displayed as functions of energy at a finite three–momentum of 100 MeV. The corresponding antikaon propagator G_K is shown in the lower panel. The figure displays the typical properties of the antikaon when it is modified by the scattering processes in the medium.

The main peak of the spectral function (the imaginary part of G_K) is shifted to lower energies compared with its vacuum position at $\omega = \sqrt{m_K^2 + k^2} \simeq 505$ MeV. However, this mass shift is not dramatic. A much stronger effect is the broadening. Taking the full width at half maximum, the antikaon is "spread" over roughly 130 MeV.

In this section we want to investigate in some more details which are the main physical sources for this behavior and how this depends on the kaon–momentum and on the density of the surrounding medium. We thereby concentrate on symmetric nuclear matter. Asymmetric matter will be discussed in Sect. 4.

3.1 Effect of selfconsistency

In this subsection we briefly discuss the relevance of finding a selfconsistent solution, rather than dressing the kaon perturbatively. Technically, once the selfconsistency calculation is set up and stable, the procedure works very well, converging after 3–4 iterations.

The effect of the selfconsistency iterations on the $\overline{K}N$ scattering amplitude is shown in Fig. 3 where the imaginary parts of T_{KN} for vanishing three–momentum and densities

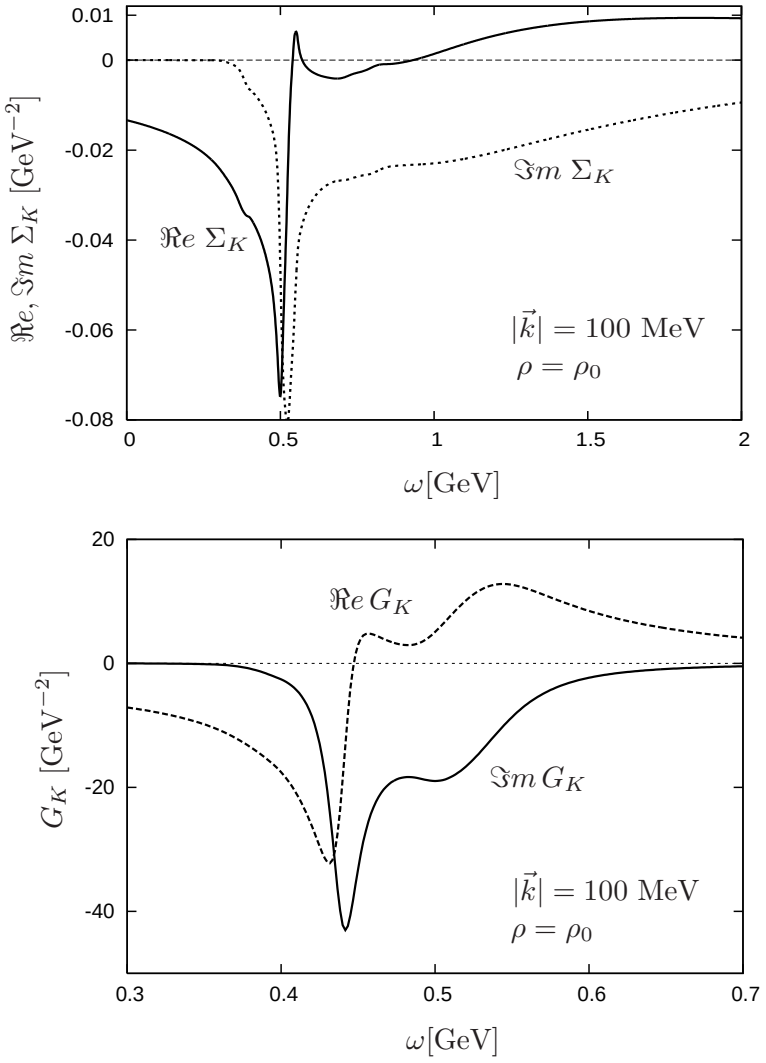

Figure 2: Real part (solid) and imaginary part (dotted) of the antikaon selfenergy (upper panel) and antikaon propagator (lower panel) as functions of energy ω at a three–momentum of $|\vec{k}| = 100$ MeV and a density of $\rho = \rho_0$.

$\rho = \rho_0$ (upper panel) and $5\rho_0$ (lower panel) are plotted as a functions of the total energy. For comparison we also show the vacuum result (dotted lines). Here one can clearly see the $\overline{K}N$ threshold at 1.43 GeV and the $\Lambda(1405)$ resonance below threshold. When the density effects are included by taking into account the Pauli blocking of the nucleon but using the unmodified kaon propagator one arrives at the dashed lines. Because of the Pauli blocking the $\overline{K}N$ threshold is shifted to higher energies and, as a result, the $\Lambda(1405)$ is also pushed upwards.

However, in the selfconsistent calculation (solid lines in Fig. 3), the change in the antikaon mass and especially the broadening of the kaon spectral function (see below) re–enables scattering into lower lying states and the resonance is pulled down again. This behavior has been discussed first in Ref. [14, 26].

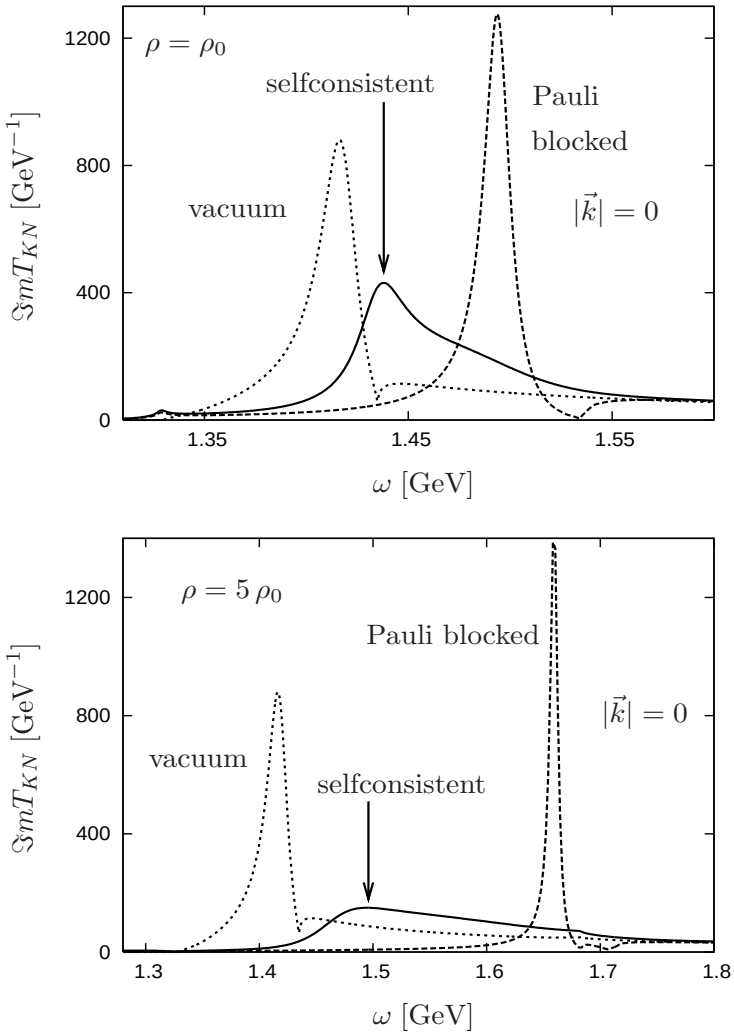

Figure 3: Imaginary part of the T–matrix $\Im m T_{\overline{K}N}$ at $|\vec{k}| = 0$ as a function of energy. Upper panel: $\rho = \rho_0$, lower panel: $\rho = 5\,\rho_0$. Dotted lines: vacuum result, dashed lines: in–medium result, only Pauli–blocking, solid lines: result after selfconsistency is reached.

Fig. 4 shows the corresponding effect of the selfconsistency iteration on the antikaon propagator (imaginary part) at $\rho = \rho_0$ and two different 3–momenta. Again, the dashed lines, labeled "Pauli–blocked", mark the results after the first iteration step, i.e., when only the Pauli–blocked T–matrix elements (cf. dashed lines in Fig. 3) are used in the selfenergy integrals. The selfconsistency iterations broaden the antikaon and shift it further down (solid line).

Also note that in the "Pauli–blocked" calculation there is a double peak structure in $\Im m G_{\overline{K}}$ which becomes more prominent at higher momentum. This feature is largely washed out by the selfconsistency iterations.

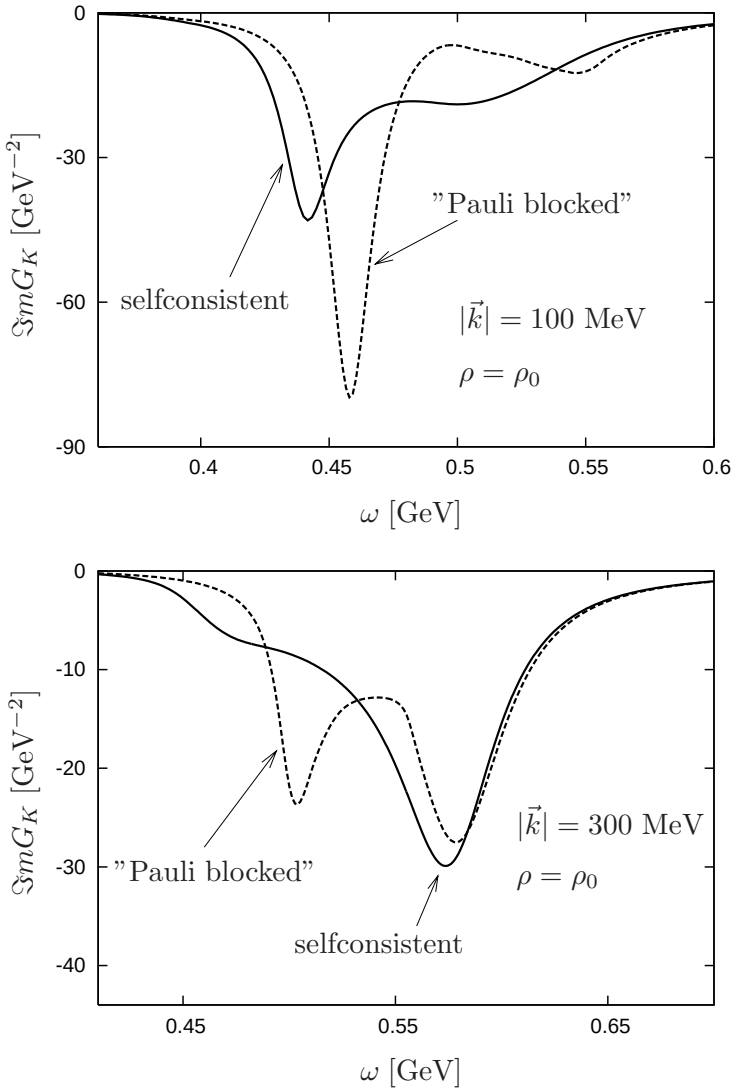

Figure 4: Imaginary part of the antikaon propagator $\Im m G_K$ at normal nuclear density $\rho = \rho_0$ as functions of energy. Upper panel: $|\vec{k}| = 100$ MeV, lower panel: $|\vec{k}| = 300$ MeV. Dashed lines: after one iteration, solid lines: after selfconsistency is reached.

3.2 Momentum and density dependence of the antikaon propagator

Fig. 4 already indicates the structure of the antikaon spectral function as a function of momentum. This is summarized in Fig. 5 which shows the imaginary part of the kaon propagator at density $\rho = \rho_0$ for three different 3–momenta, $|\vec{k}| = 100$ MeV, 200 MeV, and 300 MeV.

As mentioned above, one typically finds two peaks. It turns out that for low values of $|\vec{k}|$ most of the strength is contained in the lower peak (solid line). With increasing $|\vec{k}|$, this peak becomes gradually reduced while the upper peak grows (dashed line). Finally, at large momenta, most of the strength is found in the upper peak (dotted line).

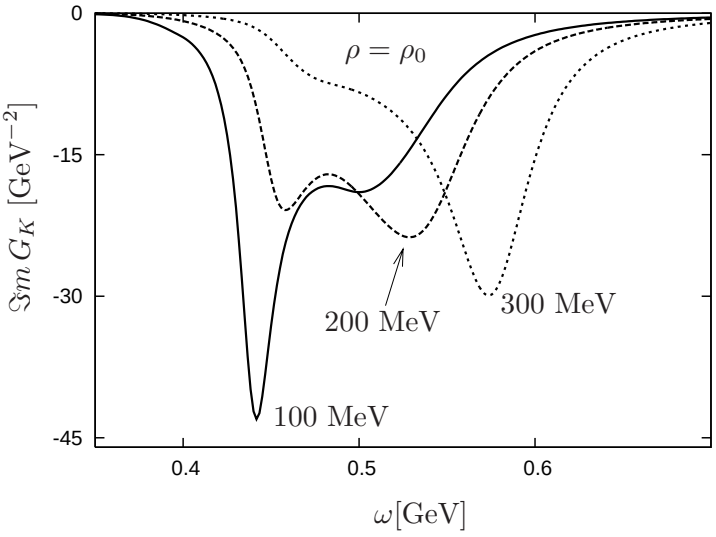

Figure 5: Imaginary part of the selfconsistent antikaon propagator at density $\rho = \rho_0$ as function of energy. The various curves correspond to three different 3–momenta: $|\vec{k}| = 100$ MeV (solid), 200 MeV (dashed), and 300 MeV (dotted).

The nature of the two–peak structure can be easily understood in terms of a simple two–level model, describing the coupling of a bare antikaon state to a $\Lambda(1405)$–hole state. At low momenta the unperturbed energies of these states are very close to each other, the $\Lambda(1405)$–hole state being only about 30 MeV below the bare kaon. However, turning on the interaction, the splitting of the peaks becomes larger through level repulsion, which shifts the "antikaon peak" somewhat up and the "$\Lambda(1405)$–hole peak" further down in energy. The latter receives most of the strength at low momenta while at large momenta the kaon branch dominates. This is quite analogous to the well–known case of a pion coupled to a Δ–hole state [43]. However, it should be noted that this picture is rather crude since, as a consequence of our coupled–channel approach, we cannot resolve the peaks in the propagator into particular quasiparticle states.

The above features of the kaon propagator are subject to a strong variation with density. This is illustrated in Fig. 6 where the imaginary part of the kaon propagator

is displayed as a function of energy at fixed 3–momentum $|\vec{k}| = 300$ MeV and the three densities $\rho = \rho_0$, $2\,\rho_0$, and $5\,\rho_0$. Obviously, the strength that at $\rho = \rho_0$ is found in the higher–lying peak is still in the lower branch at the higher densities. This behavior is consistent: At higher densities the medium modifications are stronger. Thus the effect of increasing 3–momentum as discussed above sets in only at even higher momenta.

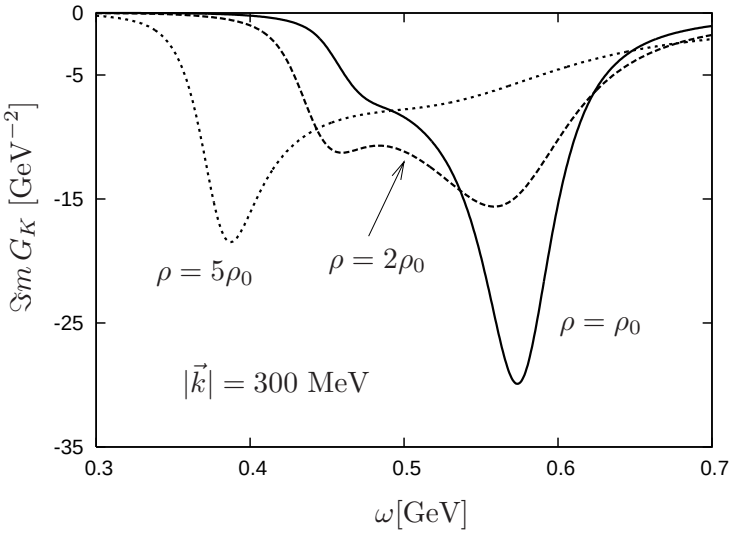

Figure 6: Imaginary part of the selfconsistent antikaon propagator at 3–momentum $|\vec{k}| = 300$ MeV. The various curves correspond to three different densities: $\rho = \rho_0$ (solid), $2\rho_0$ (dashed), and $5\rho_0$ (dotted).

At very high momenta, the free dispersion relation of the antikaon is regained. This provides some technical help, allowing the use of the free antikaon beyond $\omega = 1.5$ GeV and $|\vec{k}| = 1.2$ GeV.

3.3 In–medium modification of the pions

The importance of the pion in the $\overline{K}N$ scattering processes was already emphasized. As pointed out earlier, the pion undergoes considerable modifications when placed in dense matter. In the following, we want to study the effect of these medium modifications of the pion propagator on the kaon propagator through the coupled–channel mechanism.

Our results are summarized in Fig. 7. The pion propagator at normal nuclear matter density is displayed in the upper panel. At the indicated pion 3–momentum of 300 MeV, the broadening effect is maximal.

Typically, the broadening of the pion in dense matter has some bearing on the π–baryon loop function in the form of a bump around threshold. As an example, the central panel of Fig. 7 shows the imaginary part of the $\pi\Sigma$ channel – loop function, $\Im m J_{\pi\Sigma}$, at normal nuclear matter density and three–momentum $|\vec{q}| = 100$ MeV. The effect seems to be sizeable, the difference to the vacuum curve is quite pronounced.

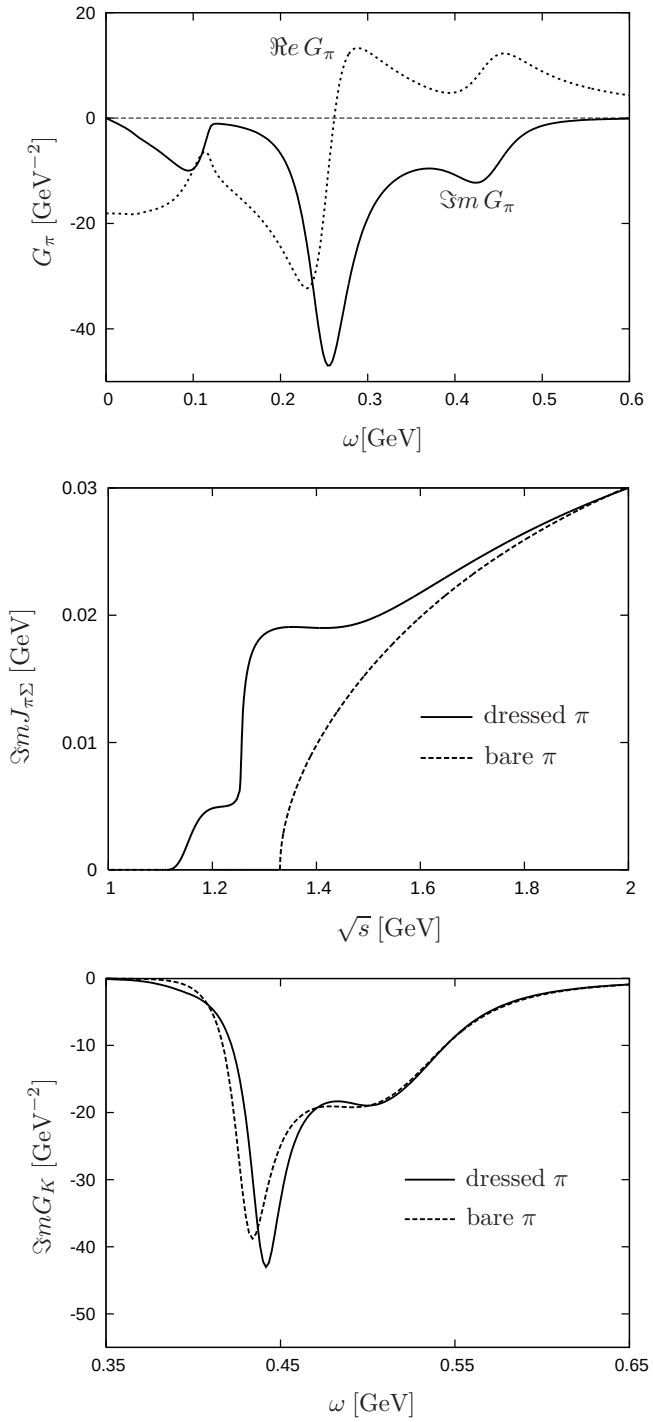

Figure 7: Upper panel: Real part (dotted line) and imaginary part (solid line) of the pion propagator at $|\vec{k}| = 300$ MeV as functions of energy.
Central panel: Imaginary part of the $\pi\Sigma$ loop function at $|\vec{q}| = 100$ MeV as function of the invariant mass, incorporating dressed (dashed line) and bare (solid line) pion propagators.
Lower panel: Imaginary part of the antikaon propagator at $|\vec{k}| = 100$ MeV as function of energy, incorporating dressed (solid line) and bare (dashed line) pions.
All calculations in this figure have been performed for $\rho = \rho_0$.

On the other hand, the lower panel indicates the difference it makes for the imaginary part of the kaon propagator, $\Im m G_{\overline{K}}$, whether the bare or the dressed pion propagator is used as input. The figure shows the selfconsistent result, again at normal nuclear matter density and $|\vec{k}| = 100$ MeV. Obviously, very little is left of the effect of pion dressing, in agreement with [47], while in [18] a stronger effect has been found. The reason is the strong momentum dependence of the pion selfenergy. At the $|\vec{k}| = 300$ MeV as in the upper panel, its effect is most pronounced. However, already the loop function (central panel) is obtained by integrating the in–medium pion over all momenta. The kaon propagator (lower panel) is the result of yet another integration – not counting the various iterations to achieve a selfconsistent result.

3.4 p–wave antikaon selfenergy

As mentioned earlier, we neglect contributions to the antikaon selfenergy arising from the p–wave vertices of Eq. (5) in our model. The reason is that these contributions are expected to be small, but would considerably complicate the selfconsistency problem.

To check the (un–) importance of the p–wave vertices for the kaon propagator, we include their contributions to the selfenergy, but only in a perturbative way. This means, we first calculate the selfconsistent kaon propagator obtained with s–wave interactions only, as before. Then we add the p–wave contributions to the selfenergy, i.e., Λ–hole and Σ–hole diagrams as depicted in Fig. 8. As in the pion case we use a monopole form factor with $\Lambda = 550$ MeV. For the Migdal parameters we take the classical value of $g' = 1/3$. The resulting total selfenergy is then used to calculate the modified kaon propagator, but the procedure is not iterated again.

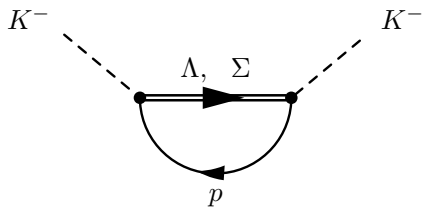

Figure 8: Diagrams corresponding to the p–wave contribution to the antikaon selfenergy.

The result for $\rho = \rho_0$ and $|\vec{k}| = 400$ MeV is shown in Fig. 9. Although the chosen three–momentum roughly corresponds to the value where the p–wave effect has its maximum, it is obviously very small. This is due to the position of the p–wave selfenergy at very low energies. In fact, it lies entirely in the space–like region. Thus the kaon with its bare pole at $\omega \sim 600$ MeV does not feel much of the p–wave selfenergy. Hence, even though somewhat larger effects have been found when the p–wave interactions are included in the meson–baryon scattering equation [18, 26, 30], their negligence seems to be justified.

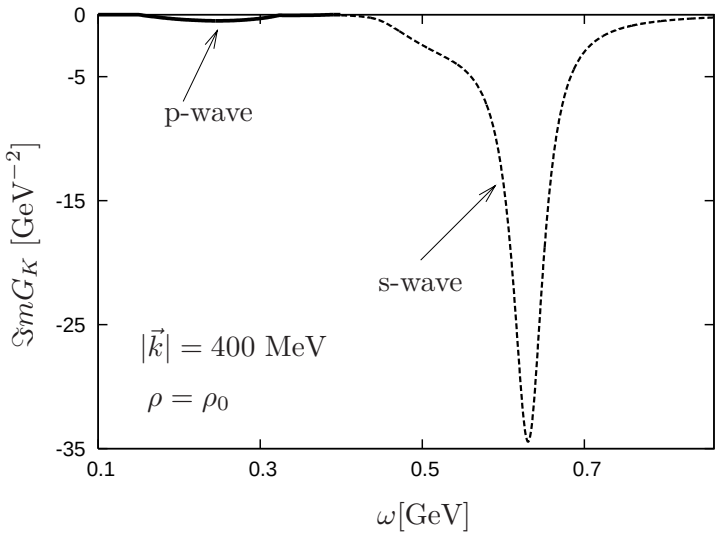

Figure 9: Imaginary part of the K^- propagator at $|\vec{k}| = 400$ MeV and $\rho = \rho_0$: s–wave (dashed) and p–wave (solid) contributions.

4 Asymmetric nuclear matter

In this section we extend our discussion to isospin asymmetric matter, i.e., to the case of unequal densities of protons and neutrons. This case is relevant for the description of neutron star matter which is expected to consist of roughly 90% neutrons and 10% protons (see Sect. 5). The calculation of the $\overline{K}N$ scattering and the antikaon selfenergy in the case of asymmetric nuclear matter follows the scheme developed in the previous sections. To discuss the systematic behavior we have investigated various proton–to–neutron ratios at various densities. In this context a somewhat more precise terminology is required: The density ρ referred to is always the total baryon number density. Since we consider the zero–temperature case, $T = 0$, the only baryons occurring in sizeable number are the nucleons.[1] Of these, a fraction x_p consists of protons. The symmetric case is thus characterized by $x_p = 0.5$.

4.1 Kaons in asymmetric matter

In Fig. 10, the kaon spectral function at vanishing 3–momentum is shown for a proton fraction of 10% and three different densities. The most important difference to the symmetric case is the fact that, due to the isospin breaking surrounding, the propagators of K^- and $\overline{K^0}$ are no longer identical, but the $\overline{K^0}$ is much more affected by the dense medium. This can be explained by the fact that the Weinberg–Tomozawa term is strongest in the $\overline{K^0}n$ and K^-p channels. Therefore, since the neutron density is ten times higher than the proton density, the $\overline{K^0}$ undergoes a stronger modification, although the various contributions

[1] For a nucleon gas with 90% neutrons, the neutron Fermi energy reaches the mass of the (undressed) Λ only at $\rho = 6.7\rho_0$

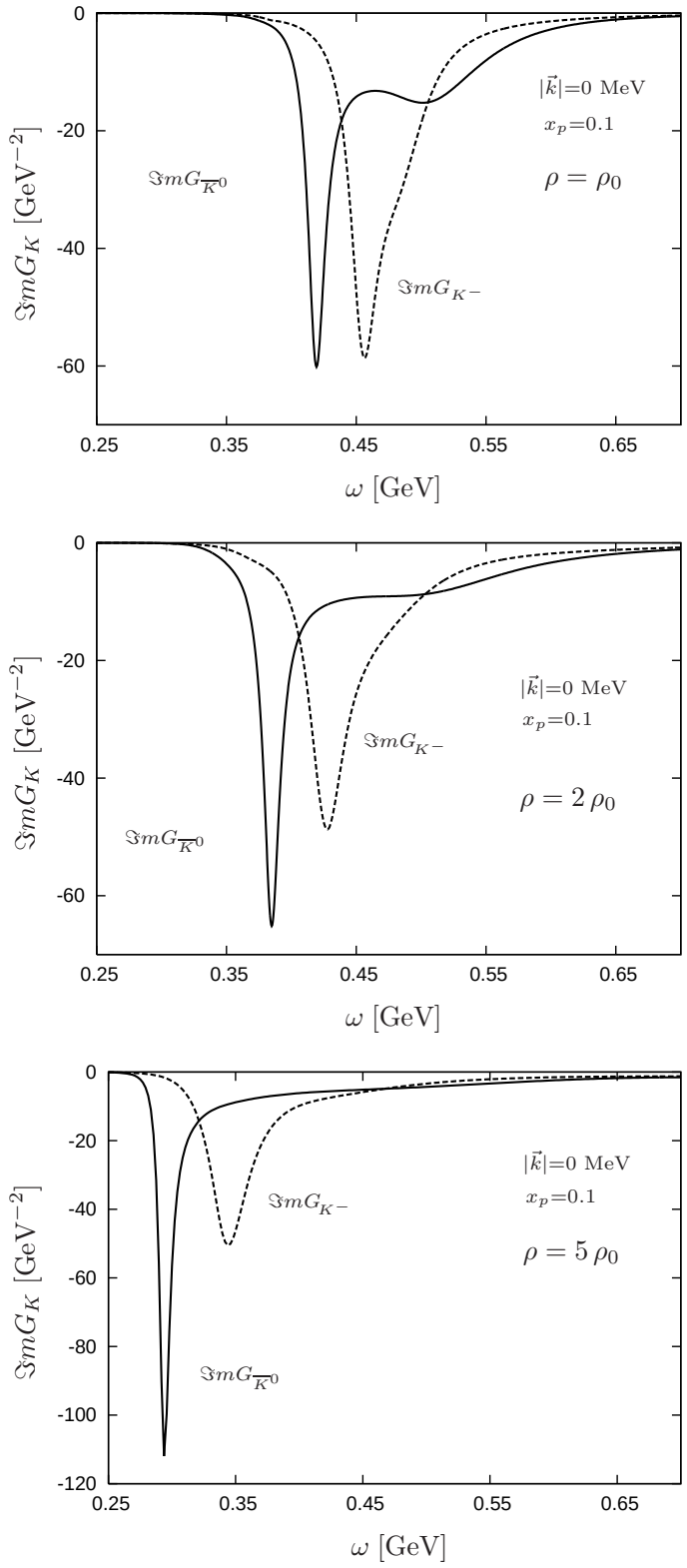

Figure 10: Imaginary parts of the K^- (solid line) and $\overline{K^0}$ (dashed line) propagators as functions of energy for $|\vec{k}| = 0$ and a proton fraction $x_p = 0.1$. Upper panel: $\rho = \rho_0$, central panel: $\rho = 2\,\rho_0$, lower panel: $\rho = 5\rho_0$.

get thoroughly mixed in the selfconsistency iterations.

The variation of $\Im m G_K$ with the proton–neutron asymmetry at different densities can be studied by comparing the curves in Fig. 11. This figure shows a smooth variation of the properties of the antikaons with density and isospin composition.

Finally, Fig. 12 shows the imaginary part of the antikaon propagator, now comparing directly the different densities, at an asymmetry of $x_p = 0.1$. As mentioned, the growing density affects the $\overline{K^0}$ much more than the K^-. However, the overall effect is not dramatic, the peaks of the spectral functions being shifted by no more than ~ 200 MeV from the vacuum positions at 500 MeV. It also becomes obvious that the width of the antikaon shrinks again at high density. This is of course an effect of shrinking phasespace.

4.2 Effect of s–wave pion–nucleon interactions

In Sect. 3.3 we have seen that the medium modifications of pions have a rather small impact on the kaon propagator in symmetric nuclear matter. We have thereby restricted ourselves to include p–wave pion–nucleon interactions, as outlined in Sect. 2.4. However, there are also known s–wave interactions which we have neglected so far. The contribution of the Weinberg–Tomozawa term to the s–wave pion selfenergy is usually held responsible for the existence of deeply bound pionic states in heavy nuclei [48]. The complete expressions for asymmetric matter in two–loop chiral perturbation theory are given by a calculation by Kaiser and Weise [49]. Their analytic expressions depend mainly on the difference of neutron and proton Fermi momenta, which means that the s–wave selfenergy is especially important in isospin asymmetric matter.

It is therefore appropriate to check the influence of s–wave pion–nucleon interactions in the context of asymmetric nuclear matter. To that end we employ the results of Ref. [49] to calculate the pion selfenergy. The effect on the π^-–propagator is illustrated in the upper panels of Fig. 13 for asymmetric nuclear matter with 10 % protons at a total density of $2\rho_0$. We see that the π^- is pushed upwards in energy, i.e., the s–wave selfenergy is repulsive here.

However, we find again that the impact of the s–wave pion selfenergy on the antikaon propagator is rather weak. The lower panels of Fig. 13 show the K^- propagator after the first iteration when the pions in the underlying πY loops are modified by p –wave and $s+p$ –wave interactions. We infer from the figure that the s–wave π–selfenergy has some bearing on the antikaon propagator, but it is quite small. The zero of the real part of G_{K^-} (the in–medium antikaon mass) is shifted upwards by just a few MeV (right panel in Fig. 13).

Thus the pion modifications in general have only minimal impact on the in–medium kaon.

5 The kaon mass under neutron star conditions

As mentioned in the Introduction, particular interest in the properties of antikaons in dense nuclear matter is caused by the possibility of kaon condensation in neutron stars [2, 3].

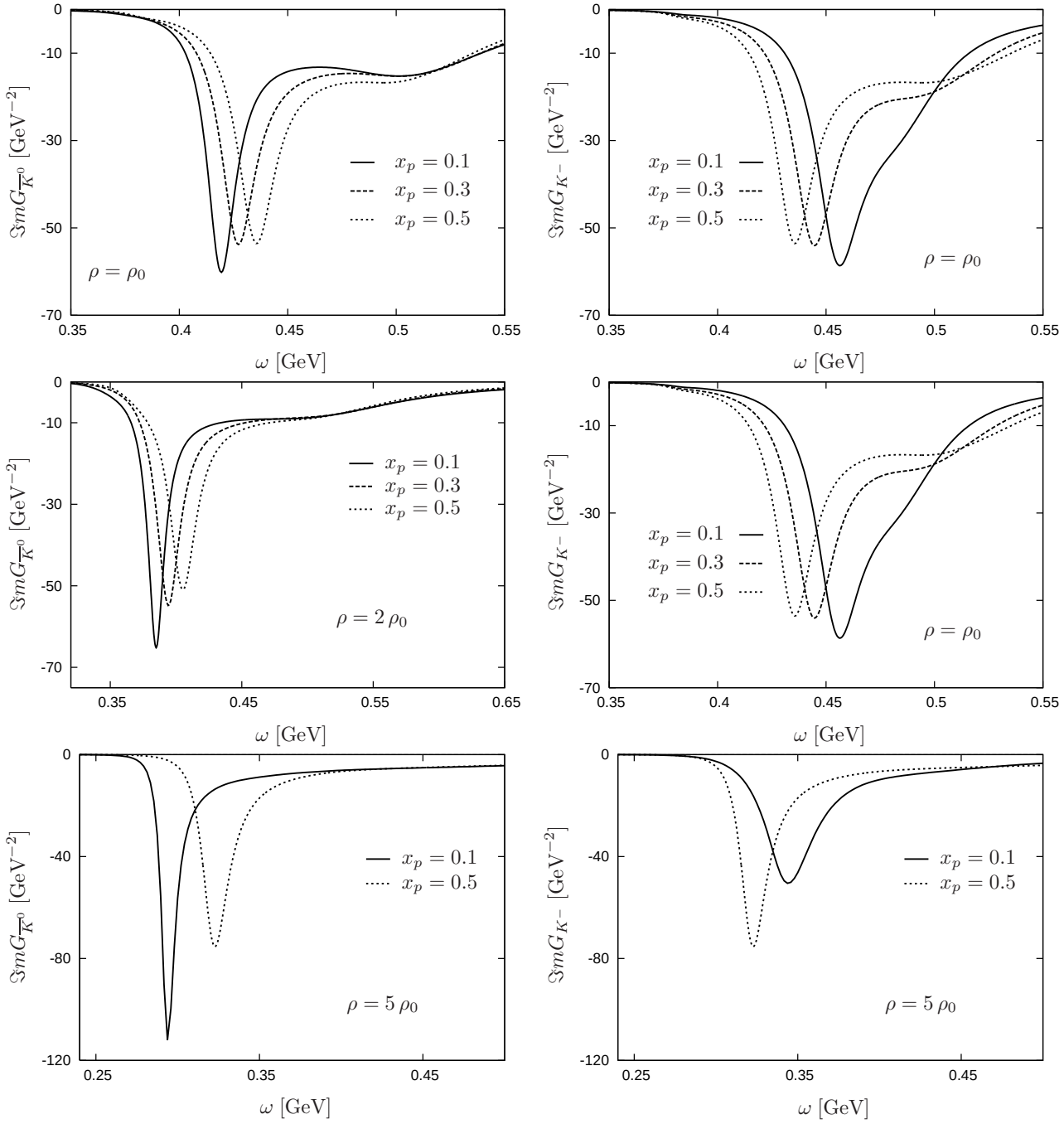

Figure 11: Imaginary parts of the propagators of $\overline{K^0}$ (left panels) and K^- (right panels) as functions of energy at $|\vec{k}| = 0$ for different baryon densities and different proton fractions.

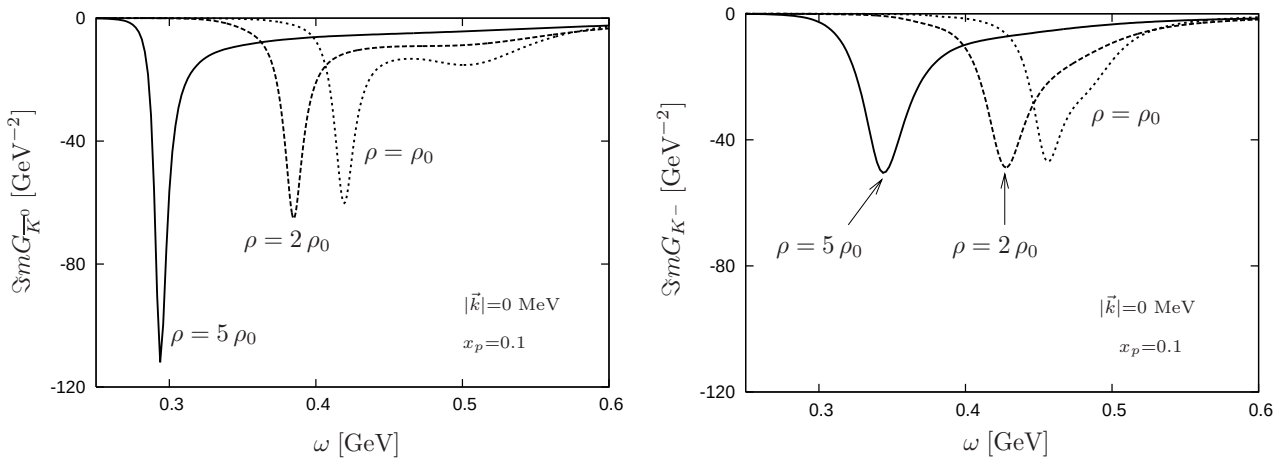

Figure 12: Imaginary parts of the antikaon propagators as functions of energy at $x_p = 0.1, |\vec{k}| = 0$ for different densities. $\overline{K^0}$ on the left, K^- on the right.

At not too high densities, neutron star matter consists of neutrons, protons, and electrons which are maintained in beta equilibrium through processes like $n \to p + e^- + \bar{\nu}_e$ and $p + e^- \to n + \nu_e$. For neutron stars older than a few minutes, the temperature is practically zero on the nuclear scale, and the neutrino mean free path is larger than the radius of the star, such that neutrinos can freely leave the system. Hence, the electron chemical potential is equal to the difference between the chemical potentials of neutrons and protons, $\mu_e = \mu_n - \mu_p$. Moreover, neutron star matter has to be electrically neutral. In the above case, this means that the densities of electrons and protons must be equal, $\rho_e = \rho_p \equiv x_p \rho$. Employing realistic equations of state, one typically finds $x_p \simeq 0.1$ (see below). For the electron chemical potential, this roughly translates into $\mu_e \simeq 150$ MeV $(\rho/\rho_0)^{1/3}$.

With increasing density, various other weak processes may become energetically possible, leading to the occurrence of new particles. In fact, according to the estimate above, already at $\rho = \rho_0$, μ_e is well above the muon mass, and the conversion $e^- \to \mu^- + \overline{\nu}_\mu + \nu_e$ should lead to a finite density of muons. At higher densities, strangeness–changing reactions should also occur. For instance, nucleons from the top of their Fermi seas could convert into hyperons.

Similarly, electrons and muons could convert into kaons,

$$e^- \to K^- + \nu_e \ , \qquad \mu^- \to K^- + \nu_e \ , \tag{17}$$

once the electron (= muon) chemical potential exceeds the in–medium mass of the K^- [50, 51, 52]. This is the case we are interested in. Obviously, the conversion of electrons and muons to kaons would reduce the number of fermions and thus their contribution to the pressure. On the other hand, the kaons might form a condensate at zero momentum that just provides a background of negative charge but, as a condensate of bosons, does not exert a degeneracy pressure. In addition, processes like $n \to p + K^-$ would increase the proton fraction in the system. Since the isospin–asymmetry part of the nuclear interaction is repulsive, this would cause a further decrease of the pressure. Thus the formation of a condensate could considerably soften the nuclear equation of state [28, 50]. In Ref. [53],

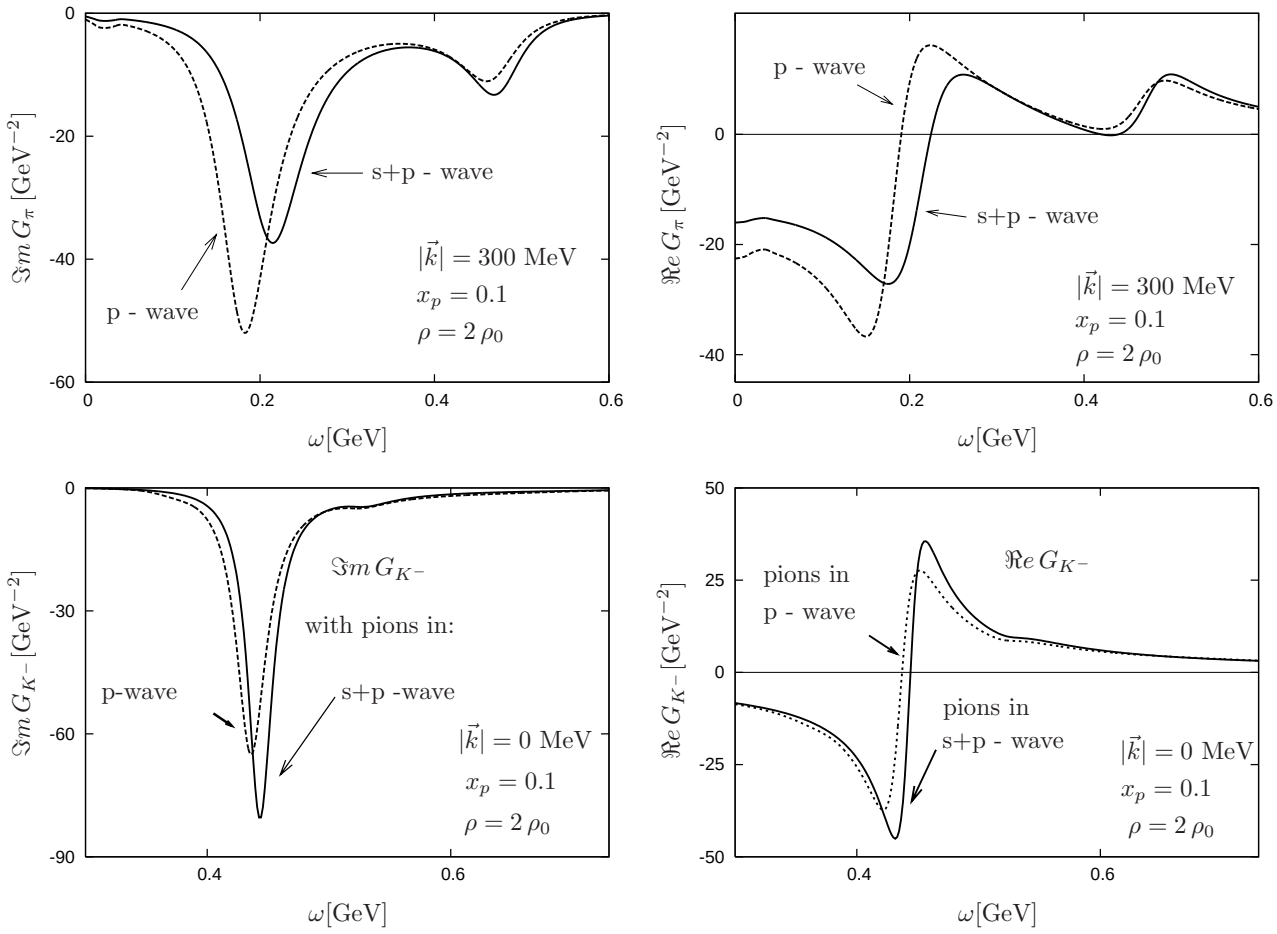

Figure 13: Upper panel: Imaginary (left) and real part (right) of the π^- propagator as functions of energy for $|\vec{k}| = 300$ MeV. Solid lines: results including s–wave and p–wave contributions, dashed lines: p–wave only.
Lower panel: Imaginary (left) and real part (right) of the K^- propagator after the first iteration as functions of energy at $|\vec{k}| = 0$, containing pions with including s–wave and p–wave selfenergies (solid line) and p–wave selfenergy only (dashed line).
All calculations in this figure correspond to total baryon density $\rho = 2\rho_0$ and proton fraction $x_p = 0.1$.

this effect has been employed to predict a maximum mass for neutron stars (better: nucleon stars) of about 1.5 solar masses and, as a consequence, the existence of a large number of low–mass black holes in our galaxy.

As pointed out above, a precondition for the conversion processes Eq. (17), is that the electron chemical potential must exceed the in–medium kaon mass, $m^*_{K^-}$. Strictly speaking, the relevant quantity is not the mass, but the energy of the kaon. However, as we have seen in Sect. 3.4, p–wave contributions to the kaon self–energy are small, and therefore the lowest energies are found at vanishing 3–momenta where they can be identified with the mass. Since the vacuum mass is much too large to be reached by μ_e at any realistic density, the question whether or not kaon condensation takes place in compact stars obviously depends crucially on how fast $m^*_{K^-}$ drops as a function of density. In the following we want to investigate this point with our model.

The mass of a given (quasi–) particle can be defined by the poles of the propagator. As explained above, we can restrict ourselves to the case of vanishing 3–momentum. We also ignore the imaginary part of the selfenergy at this stage and postpone its discussion to the end of this section. Then, the in–medium kaon mass is given by

$$\Re e\, G^{-1}_{\overline{K}}(\omega = m^*_K, \vec{k} = 0) = \omega^2 - m^2_K - \Re e\, \Sigma_{\overline{K}}(\omega, \vec{k} = 0)\Big|_{\omega = m^*_K} = 0 \tag{18}$$

Alternatively, we could define the mass as the maximum of the spectral function. It turns out that the difference between these two definitions is small for the cases of interest.

As we have seen in Sect. 4, the kaon propagator depends on both, total density ρ and proton fraction x_p of the surrounding medium. Hence, in order to proceed, we have to know x_p as a function of ρ. For neutron star matter this is in principle fixed by the requirement of beta equilibrium and neutrality. However, to apply these conditions, we need to know the equation of state which determines the relation between chemical potentials and densities of the involved particles. As for the leptons, we can safely employ ideal gas relations. On the other hand, this does not work for the hadrons where an ideal gas equation of state yields unrealistically small proton fractions. Ultimately, of course, all hadrons should be described within a unified approach, where the in–medium pions and kaons are used to calculate the dressed nucleons and vice versa. Lacking such a description at the present stage, we have consulted the literature to get some insight: In Ref. [54], Akmal and collaborators compare x_p in neutral beta–stable matter resulting from a variety of nucleon–nucleon interactions, such as the Bonn, Urbana and Argonne models as well as the Nijmegen results. Typically, the values are of the order $x_p = 0.1$, with a general tendency that x_p is rising with density. (For instance, taking their calculation based on the Argonne NN interaction v_{18} and including boost corrections (δ_ν) and a parameterization of three nucleon forces (UIX^*), one finds $x_p = 0.06$ at $\rho = \rho_0$ and $x_p = 0.14$ at $\rho = 5\rho_0$, while the v_{18} interaction alone gives just $x_p = 0.095$ at $\rho = 5\rho_0$.) In view of these and other uncertainties and the fact that our results are not extremely sensitive to small variations of x_p, we take a fixed value of $x_p = 0.1$ in our analysis.

In Fig. 14 we show the real part of the inverse kaon propagator $G^{-1}_{\overline{K}}$ at vanishing momentum 3–momentum as a function of energy. The three panels correspond to three different densities, $\rho = \rho_0$, $\rho = 2\rho_0$, and $\rho = 5\rho_0$. For completeness both the K^- (solid lines) and the $\overline{K}^0$ (dashed lines) are shown, although only the K^- mass is relevant for the

question of kaon condensation. For comparison, we also indicate the dispersion relation of the free kaon (dotted lines).

The resulting effective kaon masses are listed in Table 1. As we have seen before, the neutral antikaons (which are irrelevant in the context of kaon condensation in neutron stars) are more strongly affected by medium effects than the negative ones.

For comparison with the literature we also list the effective mass for symmetric matter. At $\rho = \rho_0$ we find $m_{\overline{K}}^{*\,symm}$= 438 MeV, corresponding to a optical potential depth of $V_{opt}^{\overline{K}} = \Sigma_{\overline{K}N}/2m_{\overline{K}}^{*} \approx -60$ MeV. This is in good agreement with [17], where $V_{opt}^{\overline{K}} \approx -55$ MeV has been extracted from an analysis of kaonic atoms.

The masses are also plotted in Fig. 15 as functions of ρ. The K^- masses are indicated by ▲ symbols. We find that the numerical results are well described by a linear fit

$$m_{K^-}^{*}(\rho) \;=\; m_{K^-}(\rho = 0)\left(1 \;-\; c\,\frac{\rho}{\rho_0}\right) \tag{19}$$

with $c = 0.06$ (solid line).

To decide whether the mass drop is sufficient to trigger kaon condensation we need to know the corresponding values of the electron chemical potential μ_e. To that end, we consider a gas of non–interacting electrons and muons and determine μ_e by requiring charge neutrality together with the protons in the system. The result is indicated by the dashed line in Fig 15. The corresponding numbers are also listed in Table 1.

Obviously, $m_{K^-}^{*}$ is well above μ_e, even at five times nuclear matter density. Even though the knowledge of nuclear interactions and the hadronic equation of state under neutron star conditions is not very good, the variations in x_p and μ_e caused by the uncertainties in present day calculations are not large enough to support the condensation scenario below $5\rho_0$. Extrapolating our results to higher densities, we predict the onset of K^- condensation at about $8\rho_0$. However, it is very unlikely that our model can be trusted up to such high densities. In the hadronic sector there are several competing channels which probably open earlier and which we have neglected so far. These could be, for instance, negative hyperons or pions. Note that each additional negative source decelerates the rise of μ_e and therefore shifts the crossing point with the kaon mass to higher densities. Eventually, a phase transition to quark matter should take place. Hence, although a more detailed investigation of all these possibilities is certainly necessary, we conclude that the occurrence of kaon condensation in neutron stars is rather unlikely.

ρ/ρ_0	μ_e [MeV]	$m_{K^-}^{*}$ [MeV]	$m_{\overline{K^0}}^{*}$ [MeV]	$m_{\overline{K}}^{*\,symm}$ [MeV]
1	141	459	420	438
2	170	430	385	407
5	221	347	294	324

Table 1: Total baryon density and corresponding values of the electron chemical potential and the in–medium masses of K^- and $\overline{K^0}$ for $x_p = 0.1$. Rightmost column: in–medium mass for $x_p = 0.5$

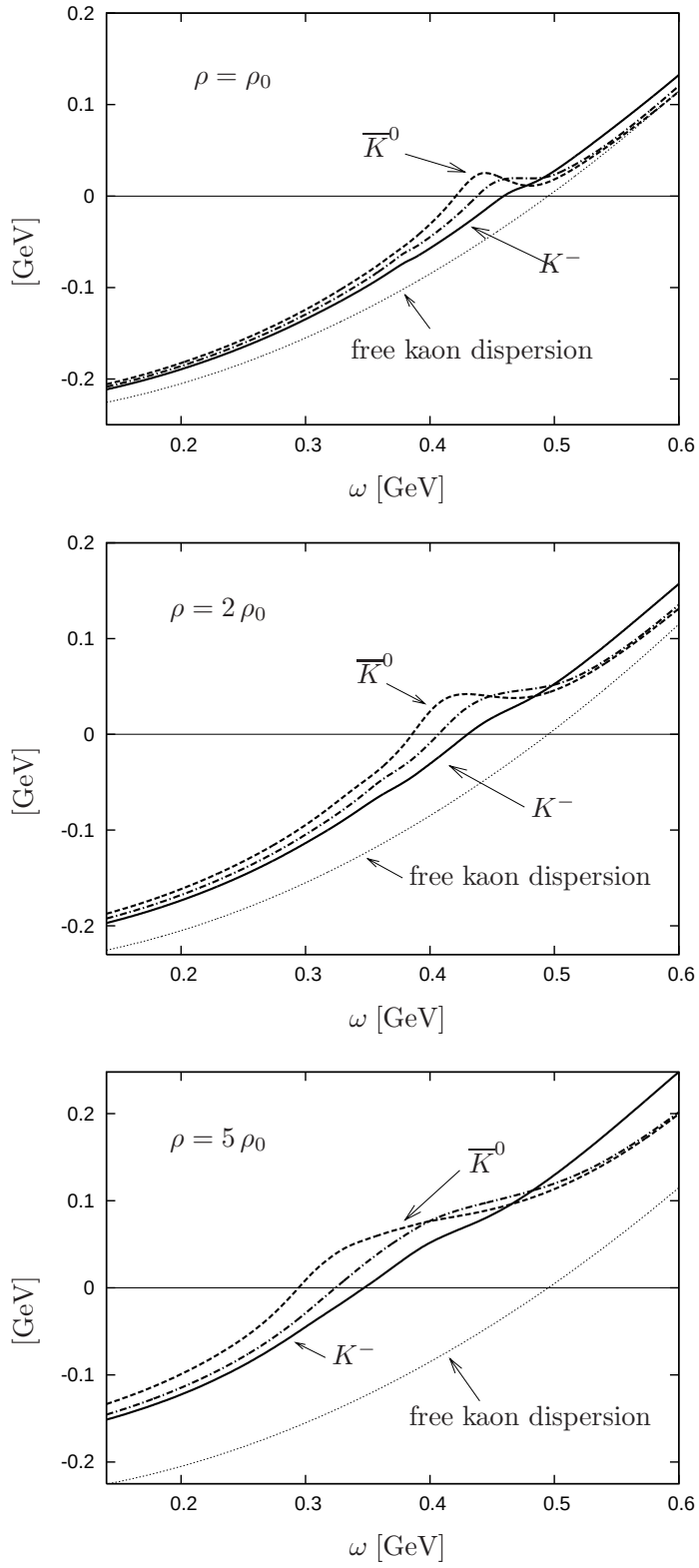

Figure 14: Real part of the inverse kaon propagator at vanishing momentum 3–momentum as a function of energy for $x_p = 0.1$ and three different densities: $\rho = \rho_0$ (upper panel), $\rho = 2\rho_0$ (center), and $\rho = 5\rho_0$ (lower panel). Solid line: K^-, dotted line: $\overline{K}^0$, dashed line: free kaon dispersion law, dashed–dotted line: $\overline{K}$ for $x_p = 0.5$

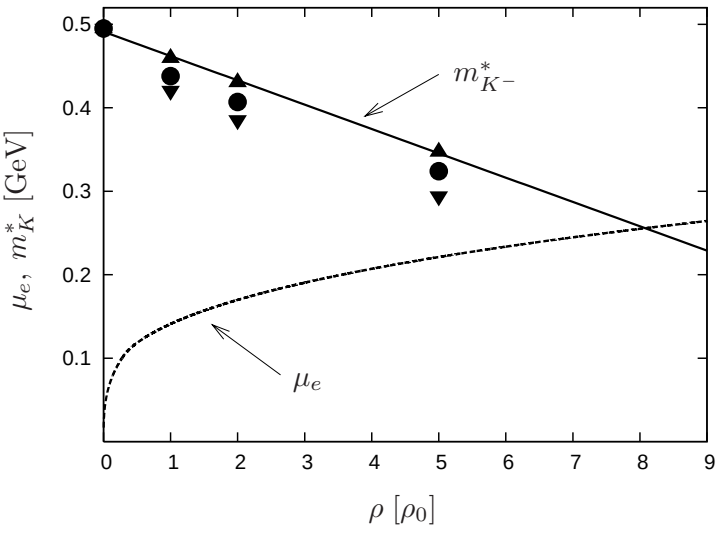

Figure 15: In–medium K^- mass $m^*_{K^-}$ (▲) and electron chemical potential μ_e (dashed line) versus baryon density at $x_p = 0.1$. The solid line represents a linear fit through the calculated points. Also indicated are the $\overline{K^0}$ mass (▼) and the in–medium mass for the symmetric case (•).

Finally, we should recall that in our determination of the in–medium kaon "mass" (cf. Eq. (18)), we have neglected the imaginary part of the selfenergy. Therefore, one might raise the question whether the consideration of the kaon width could change our conclusions. However, this seems not to be the case: As one can see in Fig. 12, even the low–energy tails of the spectral functions are far away from the values of μ_e given in Table 1.

In this context we should emphasize that our present approach is not suited to describe the phase transition to a kaon condensed phase itself. If we further increase the density, eventually part of the spectral function will move below μ_e while another part still lies above, and it would be unclear whether or not the conversion process Eq. (17) takes place[2]. This is an artifact of our model where we calculate the modified kaon propagator, leaving the ground state of the system, i.e., the Fermi sea of nucleons, unchanged. It is clear that, once kaon condensation sets in, the kaons with vanishing 3–momentum are part of the ground state, and the width of the propagator has to vanish at $\omega = \mu_e$. Hence, our present approach is only justified as long as the modifications of the nucleonic ground state are small in comparison with the kaon sector, i.e., as long as we are far away from the phase transition. In this sense, at $\rho = 5\rho_0$ we are still on the safe side.

[2]Strictly speaking, this problem exists already at lower densities in our model: If we cut the kaon selfenergy in Fig. 1, we see that there is a contribution corresponding to the decay $K^- \to \pi^0 \Lambda p^{-1}$, where p^{-1} denotes a hole state in the Fermi sea of the protons. Moreover, the pion can further decay into a nucleon–hole state. Therefore the imaginary part of the kaon propagator opens at an energy approximately equal to the Λ–proton mass difference, where we have neglected the Fermi energy of the protons. This means that part of the kaon spectral function is formally below the electron chemical potential as soon as the latter exceeds this value which is the case at about $2\rho_0$.

6 Summary

We have investigated the properties of antikaons in dense nuclear matter, focusing on the regime of zero temperature and high densities. Taking the most important KN vertices derived in χPT: the Weinberg–Tomozawa term and the σ terms, we have constructed the T–matrix for meson–baryon scattering within a coupled–channel approach, thereby dynamically generating the $\Lambda(1405)$ resonance. Regularization of the scattering amplitudes was accomplished by means of twice subtracted dispersion relations. The values of the subtraction constants have been fixed by a fit to the experimental scattering lengths.

Having developed a satisfactory description of the scattering process in vacuum, the calculations have been extended to the dense medium. The medium was treated in the nucleon gas approximation, i.e., assuming a free Fermi gas of protons and neutrons. This leads to a modified T–matrix through Pauli blocking the occupied nucleon states. On the other hand, closing a nucleon (hole) loop in the T–matrix, we obtained the in–medium self–energy of the antikaon. In turn, the resulting kaon propagator was used to (re–) calculate the T–matrix. This procedure was iterated until a selfconsistent result was achieved. Convergence was reached after some four to five iterations. The actual implementation of the selfconsistency scheme requires the determination of the scattering amplitudes and the antikaon propagator for the entire energy–momentum plane. A suitable method to implement this requirement was developed.

We first applied the model to isospin symmetric nuclear matter. We found that the $\Lambda(1405)$ resonance is moved to higher energies and becomes strongly broadened. The antikaon also receives a finite width and is mostly shifted to lower energies. Its spectral function is found to be strongly momentum dependent, emphasizing the need for a calculation that correctly incorporates the finite 3–momentum of the scattering process and the in–medium antikaon. The spectral function at zero momentum is broad but the antikaon mass still seems to be well defined. At finite but small momenta there are two branches that stem from the in–medium excitations at lower energies and the antikaon pole at $\sqrt{s} \approx 500$ MeV. At higher momenta the antikaon dispersion relation approaches its free form.

Besides the momentum dependence, we found the selfconsistent treatment of T–matrix and kaon propagator to have the largest effect on the results, while other features, like the in–medium modification of the pions and p–wave KN–interactions were found to be less important.

We then applied our model to isospin–asymmetric matter as found inside neutron stars. Although the general dependence on density and momentum is similar to that seen for symmetric matter, the most important difference is that, in asymmetric matter, K^- and $\overline{K^0}$ develop distinct spectral functions. This could be traced back to the Weinberg–Tomozawa term which is strongest in the $\overline{K^0}n$ and K^-p channels.

Finally, we investigated the possibility of K^- condensation in neutron stars. Condensation should set in when the K^- mass falls below the electron chemical potential in electrically neutral beta equilibrated matter. Neglecting the width of the K^-, we found that the mass can be described rather well by a linear fit, $m^*_{K^-}(\rho) = m_{K^-}(\rho = 0)(1 - 0.06\rho/\rho_0)$. This drop is too slow to support kaon condensation for densities up to at least $5\rho_0$.

Acknowledgments

We are grateful to M. Lutz for illuminating discussions and the possibility of comparing our vacuum amplitudes with his results. We thank M. Urban and A. Wirzba for expert advice on χPT and technical questions, and A. Gal. for instructive comments. Th. R. acknowledges support by COSY contract 41315274 (COSY–039).

References

[1] J. Rafelski and B. Müller, Phys. Rev. Lett. **48**, 1066 (1982).

[2] D. B. Kaplan and A. E. Nelson, Phys. Lett. **B 175**, 57 (1986).

[3] D. B. Kaplan and A. E. Nelson, Phys. Lett. **B 192**, 193 (1987).

[4] X. S. Fang, C. M. Ko, G. E. Brown and V. Koch, Phys. Rev. **C 47**, 1678 (1993).

[5] S. Weinberg, Phys. Rev. **17**, 616 (1966).

[6] Y. Tomozawa, Nuov. Cim. **XLVI**, 707 (1966), Serie X.

[7] H. Yabu, S. Nakamura, F. Myhrer and K. Kubodera, Phys. Lett. **B 315**, 17 (1993), nucl-th/9305008.

[8] H. Yabu, F. Myhrer and K. Kubodera, Phys.Rev. **D 50**, 3549 (1994), nucl-th/9402014.

[9] V. Thorsson and A. Wirzba, Nucl. Phys. **A 589**, 633 (1995), nucl-th/9502003.

[10] A. Wirzba and V. Thorsson, *In-medium effective chiral lagrangians and the pion mass in nuclear matter*, page 31, Proceedings of the Intl. Workshop XXVIII on Gross Porperties of Nuclei and Nuclear Excitations, Hirschegg, Austria, hep-ph/9502314.

[11] B. Krippa and J. T. Londergan, Phys. Rev. **C 58**, 1634 (1998), nucl-th/9805011.

[12] V. Koch, Phys. Lett. **B 337**, 7 (1994), nucl-th/9406030.

[13] N. Kaiser, T. Waas and W. Weise, Nucl. Phys. **A 612**, 297 (1997), hep-ph/9607459.

[14] M. Lutz, Phys. Lett. **B 426**, 12 (1998), nucl-th/9709073.

[15] E. Oset and A. Ramos, Nucl. Phys. **A 635**, 99 (1998), nucl-th/9711022.

[16] E. Friedman, A. Gal and C. J. Batty, Nucl. Phys. **A 579**, 518 (1994).

[17] A. Cieply, E. Friedman, A. Gal and J. Mares, Nucl. Phys **A 696**, 173 (2001), nucl-th/0104087.

[18] L. Tolos, A. Ramos, A. Polls and T. Kuo, Nucl.Phys. **A690**, 547 (2001), nucl-th/0007042.

[19] N. Herrmann, (FOPI Collaboration), Nucl. Phys. **A 610**, 49c (1996), nucl-ex/9610007.

[20] F. Laue et al., (KaoS Collaboration), Phys. Rev. Lett. **82**, 1640 (1999), nucl-ex/9901005.

[21] P. Senger, (KaoS Collaboration), *Strange mesons in dense matter*, in *Hadrons in dense matter*, page 96, Proceedings of the Intl. Workshop XXVIII on Gross Porperties of Nuclei and Nuclear Excitations, Hirschegg, Austria, 2000.

[22] A. Devismes, (FOPI Collaboration), *Results from FOPI on strangeness production and propagation in hot and dense nuclear matter*, in *Hadrons in dense matter*, page 104, Proceedings of the Intl. Workshop XXVIII on Gross Porperties of Nuclei and Nuclear Excitations, Hirschegg, Austria, 2000.

[23] P. Senger, (KaoS Collaboration), *Strangeness and charm production in nucleus-nucleus collisions at beam energies near the thresholds*, in *Structure of hadrons*, page 259, Proceedings of the Intl. Workshop XXIX on Gross Porperties of Nuclei and Nuclear Excitations, Hirschegg, Austria, 2001.

[24] T. Waas, N. Kaiser and W. Weise, Phys. Lett. **B 379**, 34 (1996).

[25] J. Schaffner-Bielich, V. Koch and M. Effenberger, Nucl. Phys. **A 669**, 153 (2000), nucl-th/9907095.

[26] M. Lutz and C. Korpa, Nucl. Phys. **A 700**, 309 (2002), nucl-th/0105067.

[27] E. Oset and A. Ramos, Nucl. Phys. **A 671**, 481 (2000), nucl-th/9906016.

[28] G. Q. Li, C.-H. Lee and G. E. Brown, Nucl. Phys. **A 625**, 372 (1997), nucl-th/9706057.

[29] G. E. Brown, C.-H. Lee and R. Rapp, Nucl. Phys. **A 639**, 455 (1998), hep-ph/9712017.

[30] E. Kolomeitsev and D. Voskresensky, Phys. Lett. **C 68**, 015803 (2003), nucl-th/0211052.

[31] E. Kolomeitsev, D. Voskresensky and B. Kämpfer, Nucl. Phys. **A 588**, 889 (1995).

[32] T. Muto, Nucl. Phys. **A 697**, 225 (2002), nucl-th/0103055.

[33] E. Kolomeitsev and D. Voskresensky, Phys. Rev. **C 60**, 034610 (1999), nucl-th/9808064.

[34] E. E. Salpeter and H. A. Bethe, Phys. Rev. **84**, 1232 (1951).

[35] U.-G. Meißner, Phys. Scripta **T 99**, 68 (2002), hep-ph/0201078.

[36] B. Borasoy, Eur. Phys. J. **C 8**, 121 (1999), hep-ph/9807453.

[37] B. Borasoy and U.-G. Meißner, Ann. Phys. (N. Y.) **254**, 192 (1997), hep-ph/9607432.

[38] M. Lutz and E. Kolomeitsev, Nucl. Phys. **A 700**, 193 (2002), nucl-th/0105042.

[39] H. W. Fearing, Few Body Syst. Suppl. **12**, 263 (2000), nucl-th/0006040.

[40] S. Scherer and H. W. Fearing, Nucl. Phys. **A 684**, 499 (2001), nucl-th/0006076.

[41] R. J. Iwasaki et al., Phys. Rev. Lett. **78** (1997).

[42] A. D. Martin, Nucl. Phys. **B 179**, 33 (1981).

[43] M. Urban, M. Buballa, R. Rapp and J. Wambach, Nucl. Phys. **A 641**, 433 (1998), nucl-th/9806030.

[44] M. Urban, M. Buballa, R. Rapp and J. Wambach, Nucl. Phys. **A 673**, 357 (2000), nucl-th/9910004.

[45] M. Urban, M. Buballa and J. Wambach, Nucl. Phys. **A 697**, 338 (2002), hep-ph/0102260.

[46] M. Urban, M. Buballa and J. Wambach, Phys. Rev. Lett. **88**, 042002 (2002), nucl-th/0110005.

[47] M. Lutz and C. Korpa, Acta Phys.Hung. **A22**, 21 (2005), nucl-th/0404088.

[48] H. Gilg et al., Phys. Rev. **C 62**, 025201 (2000).

[49] N. Kaiser and W. Weise, Phys. Lett. **B 512**, 283 (2001), nucl-th/0102062.

[50] A. Ramos, J. Schaffner-Bielich and J. Wambach, Lect.Notes Phys. **578**, 175 (2001), nucl-th/0011003.

[51] G. E. Brown, C.-H. Lee, M. Rho and V. Thorsson, Nucl. Phys. **A 567**, 937 (1994), hep-ph/9304204.

[52] C.-H. Lee, G. E. Brown, D.-P. Min and M. Rho, Nucl. Phys. **A 585**, 401 (1995), hep-ph/9406311.

[53] G. E. Brown and H. A. Bethe, Astrophys. J. **423**, 659 (1994).

[54] A. Akmal, V. R. Pandharipande and D. G. Ravenhall, Phys.Rev. **C 58**, 1804 (1998), nucl-th/9804027.